IOPscience iopscience.iop.org

Unconventional electroabsorption in monolayer MoS_2

This content has been downloaded from IOPscience. Please scroll down to see the full text.

View the table of contents for this issue, or go to the journal homepage for more

Download details:

IP Address: 128.179.136.173
This content was downloaded on 26/01/2017 at 15:14

Please note that terms and conditions apply.

2017 2D Mater. 4 021005

2D Materials

LETTER

Unconventional electroabsorption in monolayer MoS_2

D Vella[1,2], D Ovchinnikov[3,4], N Martino[5], V Vega-Mayoral[1,2], D Dumcenco[3,4], Y-C Kung[3,4], M-R Antognazza[6], A Kis[3,4], G Lanzani[6,7], D Mihailovic[1,2,8,9] and C Gadermaier[1,2]

[1] Department of Complex Matter, Jozef Stefan Institute, Jamova 39, 1000 Ljubljana, Slovenia
[2] Jozef Stefan International Postgraduate School, Jamova 39, 1000 Ljubljana, Slovenia
[3] Electrical Engineering Institute, École Polytechnique Fédérale de Lausanne, CH-1015 Lausanne, Switzerland
[4] Institute of Materials Science and Engineering, École Polytechnique Fédérale de Lausanne, CH-1015 Lausanne, Switzerland
[5] Wellman Center for Photomedicine, Massachusetts General Hospital and Harvard Medical School, 65 Landsdowne St, Cambridge, MA 02139, United States of America
[6] Center for Nano Science and Technology, Italian Institute of Technology, Via Pascoli 70/3, 20133 Milano, Italy
[7] Department of Physics, Politecnico di Milano, P Leonardo da Vinci 32, 20133 Milan, Italy
[8] Faculty of Mathematics and Physics, University of Ljubljana, Jadranska 19, 1000 Ljubljana, Slovenia
[9] Center of Excellence in Nanoscience and Nanotechnology, Jamova 39, 1000 Ljubljana, Slovenia

E-mail: daniele.vella@ijs.si **and** christoph.gadermaier@ijs.si

RECEIVED
4 October 2016

REVISED
6 December 2016

ACCEPTED FOR PUBLICATION
6 January 2017

PUBLISHED
25 January 2017

Keywords: electroabsorption, electromodulation, monolayer MoS_2, spectroscopy, excitons, trions

Supplementary material for this article is available online

Abstract

Signal modulation in optoelectronics is obtained by modulation of either the refractive index or the absorbance by an electric field. However, electromodulators have not kept up with the miniaturization of other electronic and optical components. Here we show a strong transverse electroabsorption signal in a monolayer of the 2D semiconductor MoS_2. The electroabsorption spectrum is dominated by an apparent linewidth broadening of around 15% at a modulated voltage of only $V_{pp} = 0.5$ V. Contrary to known variants of the Stark effect, the broadening increases linearly with the applied field strength and arises from a linear variation of the distance between the strongly overlapping exciton and trion resonances. The achievable modulation depths exceeding 0.1 dB nm^{-1} bear the scope for extremely compact, ultrafast, energy-efficient electroabsorption modulators for integrated photonics, including on-chip optical communication.

Introduction

To translate electrical into optical signals one uses the modulation of either the real or imaginary part of the refractive index of a material by an electric field. Contemporary electroabsorption modulators (EAMs) employ the quantum confined Stark effect (QCSE) [1–3], the field-induced red-shift and broadening of the strong excitonic absorption resonances characteristic of low-dimensional semiconductor structures. However, compared to the miniaturization currently happening in photonic components, EAMs remain relatively bulky and are becoming an obstacle for further photonic integration.

2D materials offer vast opportunities for photonics since they combine easy fabrication and mechanical flexibility with particularly strong light–matter interaction [4, 5]. Semiconducting 2D transition metal dichalcogenides [6, 7] such as MoS_2 support tightly bound excitons [8] with particularly strong absorption cross sections, with a monolayer absorbing about 10% of the incident light (figure 1(a)). This exceptional light–matter interaction is corroborated by cavity polaritons at room temperature [9], strong optical Stark effect [10], and ultrasensitive phototransistors [11].

Here we measure the transverse EA of monolayer MoS_2 by modulating the gate voltage V_g (with peak-to-peak voltage V_{pp}) in a transparent field effect transistor. We superimpose this modulation on a DC offset voltage, which we can choose such that the transistor is either *ON* or *OFF*. The two regimes are separated by the threshold voltage V_{th}, which is the intercept of the linear fit of the I_{ds}/V_g curve [12] ($V_{th} = 3.6$ V for Device 1 and $V_{th} = 0.55$ V for Device 2, see figures 1(d) and 2(b), inset). In the *ON* state, we measure electroabsorption together with a spectral contribution due to the modulation of the charge density (charge induced absorption). Charge induced absorption changes the population of electronic levels and thus the strength of

© 2017 IOP Publishing Ltd

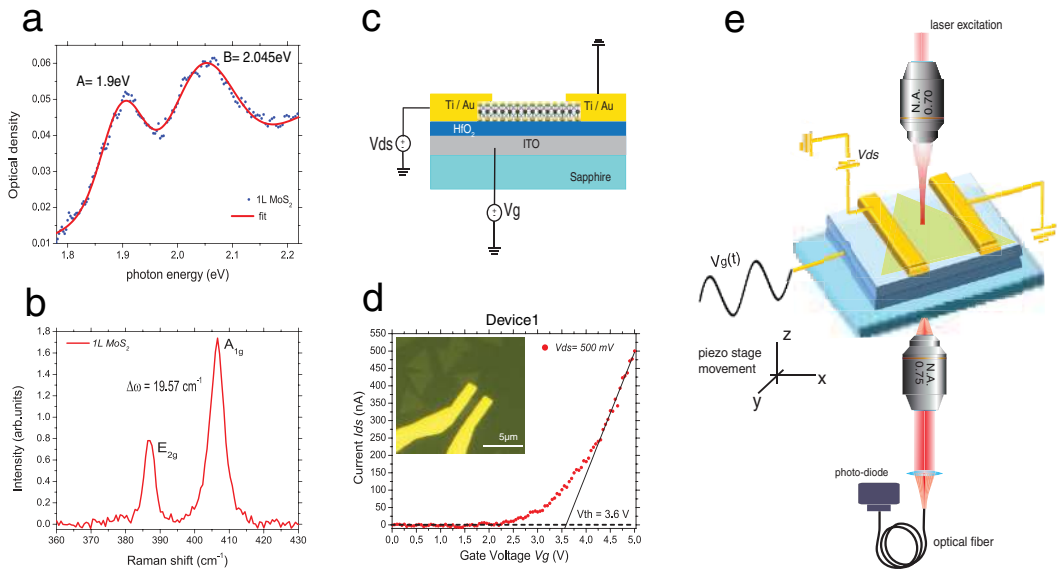

Figure 1. Optical and electrical characterisation of MoS_2 monolayer transistors. (a) Extinction spectrum of the MoS_2 monolayer. (b) Raman spectrum of the MoS_2 monolayer. (c) Schematic of the transistor geometry. (d) Dependence of the current (I_{ds}) of the gate voltage (V_g) for device 1. Inset shows an optical micrograph of the device. (e) Schematics of the extinction and electroabsorption measurements using a tuneable laser in a confocal microscope.

different spectral features, such as an enhanced absorption from charges to trions [13, 14] or a decrease of the excitonic absorption features due to phase-space filling (Pauli blocking) [15]. In the *OFF* state the charge density in the channel remains constant over the modulation period and we measure pure electroabsorption. Most experiments in the present study have been performed with the transistor in the *OFF* state. Since no charges are moved inside the device in this configuration, the EA response is not limited by the electrical response time of the transistor.

Methods

The transistor is built according to the structure in [17], using *c*-plane sapphire as the transparent substrate and 50 nm of ITO as the transparent back-gate electrode. The gate dielectric consists of 30 nm of HfO_2 deposited by atomic layer deposition; the source and drain electrodes are made of Ti/Au (5/50 nm thickness). Monolayer MoS_2 has been grown by chemical vapour deposition on *c*-plane sapphire following the method in [22]. As-synthesized MoS_2 was transferred from the sapphire to the target substrate (sapphire/ITO/HfO_2) using a wet transfer method based on a glass slide covered with Polydimethylsiloxane(PDMS) as a stamp, a poly(L-lactic acid) polymer film (PLLA) as the holder for the flakes and deionized water promoting the detachment of the polymer. Successively the stack PDMS/PLLA/MoS_2 was placed in a homemade transfer station setup and vertical aligned with the target. After approaching the target substrate, the system PDMS/PLLA/MoS_2/target (all in contact with each other) was kept at 100 °C for 2 h to allow a better adhesion of the flakes. The transfer was carried out with the following cleaning procedure (see suppl. info (stacks.iop.org/TDM/4/021005/mmedia)): 1 h in dichloromethane (PLLA solvent) that allows the separation of the target + flakes from the glass + PDMS stamp, bath of the chip in acetone (1 h) and in isopopanol (2 h), drying in N_2 for each step. Final annealing at 250 °C in low vacuum (10^{-2} mbar) for 6 h at 250 °C in a flow of argon gas (200 sccm). Finally the process was completed by electron beam lithography. The transistor transfer characteristic recorded in air (figure 1(d)) shows a turn on voltage V_{on} that varies with time from a positive voltage near 0 V towards values around 2.5 V (figure 1(d), insert figure 2(b)). This indicates *p*-doping from atmospheric adsorbates onto the FET channel.

The EA data were collected with a homemade confocal microscope in transmission configuration. The light source consisted of a supercontinuum laser (NKT Photonics, SuperK Extreme) monochromated by an acousto-optic modulator (NKT Photonics, SuperK Select) in the 500–1000 nm region with line widths between 2 and 5 nm. The polarization of the laser was then controlled with a half-wave plate and a linear polarizer. The light was then focused on the device with a 0.7 N.A. objective (S Plan Fluor 60×, Nikon) and collected by a second 0.75 N.A. objective (CFI Plan Apochromat VC 20×, Nikon). The collected light was focused on the entrance of a multimodal glass fiber with a 50 μm core, acting as confocal aperture and revealed by a silicon photodetector (FDS100, Thorlabs). The signal was amplified by a transimpedance amplifier (DHPCA-100, Femto) and supplied both to a DAQ (to record the transmission signal, T) and to a lock-in amplifier (SR830 DSP, Stanford Research Systems) to retrieve the differential transmission data, ΔT. All data were collected by a custom Labview Software that also

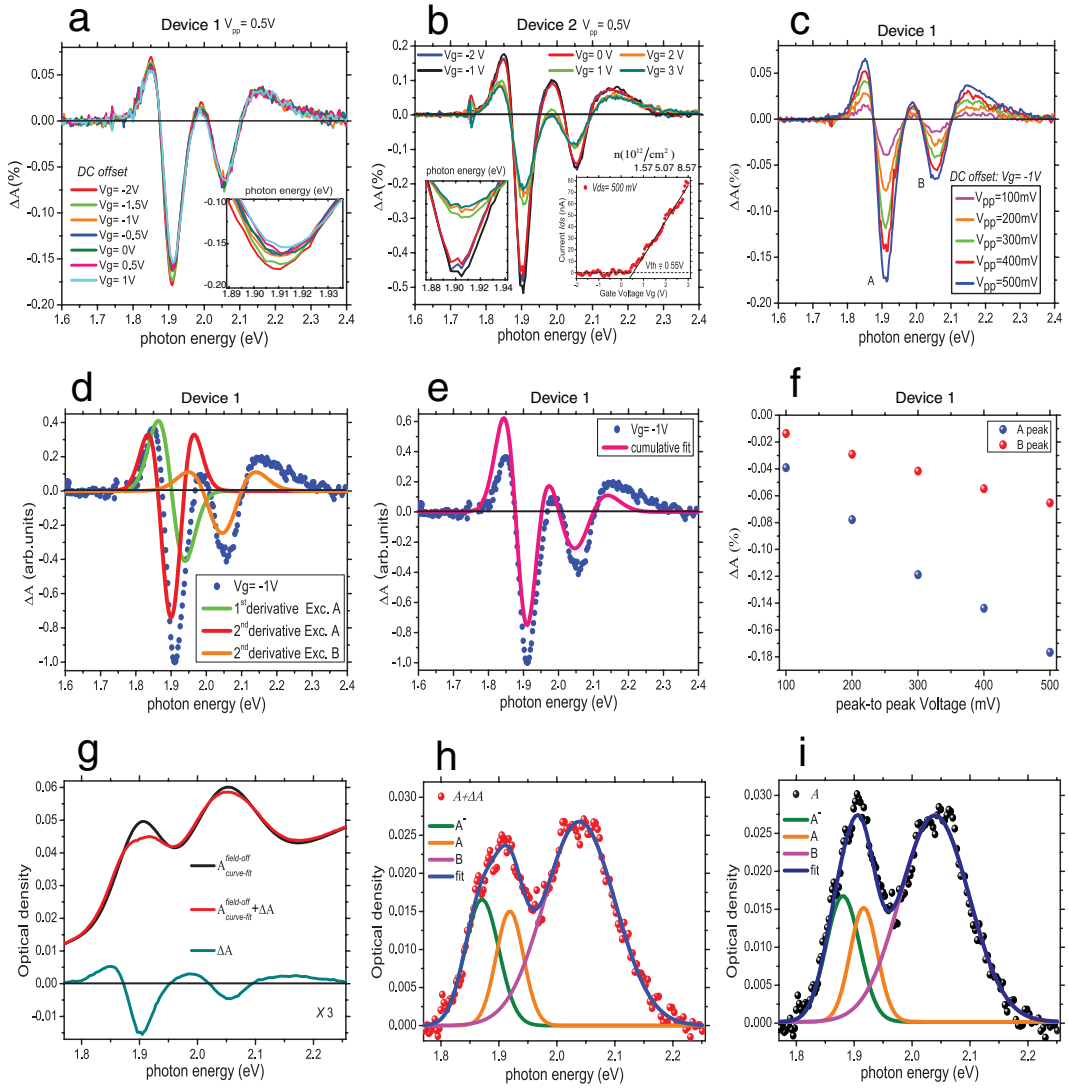

Figure 2. Electroabsorption spectra of MoS_2 monolayer transistors. (a) and (b) Electroabsorption spectra of devices 1 and 2 for different gate voltage DC offsets. Insets show zoom into the main peak for better distinction of the individual lines. Inset in (b) shows the gate voltage dependence of the current in device 2. (c) Electroabsorption spectra of device 1 for different peak-to-peak voltage modulation amplitude V_{pp}. (d) and (e) Normalised electroabsorption spectrum (dotted) of device 1 and first and second derivatives of the absorption peaks used to fit the spectra (individual contributions in d, cumulative fit in (e). (f) *A* and *B* peak amplitudes from (c) as a function of V_{pp}. (g) Fit of the extinction spectrum (black), electroabsorption spectrum (cyan) and sum of the two (red) give the extinction spectrum at a gate voltage $V_g = V_{pp}$. (h) and (i) Extinction spectra with and without field fitted to three Gaussian curves.

controlled the raster scan of the device via a 3D piezo stage (P-517, Physik Instrumente) and the laser system. The laser fluence is kept below 150 W cm^{-2} to avoid photodoping [21].

Results

The absorption spectrum of MoS_2 in figure 1(a) shows the characteristic *A* and *B* exciton resonances [4–11]. The distance between the two main Raman peaks in figure 1(b), $\Delta\omega = 19.6\,cm^{-1}$ confirms the monolayer thickness [16]. The transistor is built in a bottom-gate configuration according to the structure in [17], using 30 nm of HfO_2 as gate dielectric and a sapphire slice as the transparent substrate (figures 1(c) and (d)). We present data from two geometrically identical devices with different turn-on voltages (figures 1(d) and 2(b)), which we ascribe to adsorption doping [18] since the measurements are carried out in air. We apply a modulated gate voltage (with peak-to-peak voltage V_{pp}) superimposed on a DC offset to the transistor and detect the change ΔT in the transmitted light intensity via a lock-in amplifier locked to the modulation frequency ω. Transmission is measured using a tuneable laser focussed on a <500 nm spot in a confocal microscope [19, 20] (figure 1(e)). We normalise the modulated signal ΔT by the transmitted light intensity T, which directly yields the change ΔA in absorbance:

$$\Delta A = -\frac{\Delta T}{T} \qquad (1)$$

The EA spectrum of monolayer MoS_2 for transverse field modulation consists of alternating positive and negative absorption changes (see figures 2(a)–

(c)), three peaks of increased absorption and two of decreased absorption. The two peaks of decreased absorption are stronger than the other three and peak at the same wavelengths as the *A* and *B* features in the absorption spectrum. The shape and magnitude of the EA signal is independent of the DC component of the gate voltage when the transistor is in the *OFF* state. When the transistor is *ON* and charges are injected, the signal is weaker and slightly changes shape. The injected charges may partly screen the field and weaken the EA signal (see the section 'electrostatic considerations' for an estimate of the screening). Moreover, in this case the modulated field also modulates the charge concentration in the channel, which adds to ΔA (charge induced absorption, see the supplementary information, figure S7) [13–15].

The most common features of EA are (i) field-induced changes in the peak positions of the *A* spectrum (red- or blue-shifts), (ii) field-induced changes in the peak width of *A* (usually broadening), and (iii) in some cases also changes in the area under the *A* curve in a certain spectral window (transfer of oscillator strength between different electronic transitions) [1, 2]. In the ΔA spectra these features appear as distinctive shapes related to the respective absorbance peaks: (i) as a first derivative of the absorbance for shifts of *A*: $\Delta A \propto \mathrm{d}A/\mathrm{d}E$, (ii) as a second derivative for changes in the width of an *A* peak: $\Delta A \propto \mathrm{d}^2A/\mathrm{d}E^2$, and (iii) as the same lineshape as the absorbance for transfer of oscillator strength: $\Delta A \propto A$. We fitted the absorption spectrum in figure 1(a) using two Gaussian peaks and a generic exponential function to account for the background from various scattering mechanisms. To identify the main contributions to the EA spectra, we used first and second derivatives of these Gaussians independently to fit the EA spectra, as shown in figures 2(d) and (e). Second derivatives dominate the ΔA spectrum, together with a first derivative contribution. Hence the main effect of the electric field on the absorbance *A* is broadening (about 6% for the *A* peak of device 1, 15% for device 2), accompanied by a slight red shift. Transfer of oscillator strength is not needed to fit the EA spectra. The joint action of broadening and red shift slightly slants the two negative peaks of the EA spectrum towards higher energies compared to the absorption resonances and diminishes the middle peak due to the overlap of positive and negative signal components.

For different modulation voltages V_{pp}, the EA signal retains its shape and increases linearly in magnitude (figures 2(c) and (f)). This means that in particular the broadening of the absorbance increases linearly with the modulated field, an unconventional behaviour that has not been reported in other materials so far. On the other hand, shifts of the absorbance with linear field dependence are common and indicate built-in fields or permanent dipole moments [22]. In engineered 2D semiconductor structures (quantum wells or multiple quantum wells), the QCSE yields a red shift proportional to the square of the applied electric field [1, 2], accompanied by a broadening of the excitonic resonances. The broadening is ascribed to an increased homogeneous linewidth due to field-induced exciton dissociation (charge transfer into the 'walls' of the quantum well), and has a highly non-linear field dependence. Hence our results disagree with the conventional QCSE. Other possible origins of the signal, such as heating or strain-induced shifts from piezoelectricity are also ruled out from their field dependence in a detailed discussion in the Supplementary Information.

Discussion

Origin of the electroabsorption signal

To explain the unconventional linear field dependence of the broadening, we take a closer look at the linewidth of the absorption resonances. Since MoS_2 from any synthesis method is doped [17, 23], the absorption peak *A* consists of at least two overlapping electronic resonances, A^0 from the neutral ground state to a neutral exciton state, and A^- from a charged ground state to a charged exciton state (trion) [13]. Similarly, the broader *B* peak should also be composed of two peaks B^0 and B^-. Although *B* trions have not been studied in detail yet, they play a role in the transient absorption spectra observed in femtosecond pump-probe experiments [24]. Since positive and negative trions appear at almost the same spectral position [25], the following considerations can also be made for *p* doping. The distance between A^0 and A^- changes almost linearly with V_g over a wide range of gate voltages comprising both the *ON* and *OFF* states [14, 24]. This shift of both features has been tentatively ascribed to Stark effect [24] or to a renormalization of both the band gap and the exciton (or trion) binding energy [14]. The latter explanation is applicable only for the *ON* state of the transistor, where the gate voltage actually modulates the charge density. Here, in the *OFF* state the charge density in the MoS_2 channel stays constant; hence we continue to discuss our results without assuming charge-density related renormalizations.

By adding the field-induced absorbance change ΔA to the absorbance *A* without field in figure 2(g) (to reduce noise, we used the fit for *A* rather than the original data) we obtain the shape of the absorbance spectrum in the presence of an electric field corresponding to a $V_g = V_{pp} = 0.5$ V. Clearly, the *A* peak is lowered and broadened and its composition by two peaks is now more clearly visible. A similar but smaller effect is also seen for peak *B*, which should also be composed of two resonances B^0 and B^-. However, peak *B* is too wide to yield accurate parameters for two component peaks; hence we do not explore its composition further. In figures 2(h) and (i) we show fits of *A* and $A + \Delta A$ using two Gaussians for peak *A*, with height and width unchanged between both cases, only different positions. This fit embodies a model where the A^0 and A^- resonances maintain their width and oscillator strength, but change their positions as a consequence

of the applied electric field. The constant height of both peaks means that no oscillator strength is transferred and, more importantly, no charge is injected into or extracted from the channel. A gate voltage of $V_g = 0.5$ V increases the distance between the A^0 and A^- peaks from 36 to 48 meV, resulting in both a broadening and lowering of the A peak as a whole. Additionally, the peak shifts slightly to the red since the red shift of the A^- peak is stronger (−9 meV) than the blue shift of the A^0 peak (+3 meV). While the composite A peak with 36 meV between the A^0 and A^- peaks (figure 2(i)) still looks very similar to a Gaussian, at 48 meV it does not (figure 2(h)), which explains why the fit with first and second derivatives of a Gaussian deviates from the real data (figure 2(e)). Note also that, to merge into what appears as one B peak, its constituent peaks B^- and B^0 must be broader than A^0 and A^-. Hence, if B^- and B^0 shift by a similar amount as A^0 and A^-, their effect on the shape of B is weaker, which explains the lower EA signal of the B peak. In conclusion, in the regime where we do not modulate the charge density, the overall unconventional change of shape of the absorbance spectrum with a linear dependence on the transverse electric field strength originates from linear shifts of the strongly overlapping exciton and trion peaks.

Electrostatic considerations

The gate voltage V_g causes a transverse electric field in the MoS_2 monolayer

$$F = \frac{V_g}{d_M + \frac{\varepsilon_M}{\varepsilon_H} d_H} \tag{2}$$

With the indices M and H indicating the thickness d and dielectric constant ε of MoS_2 ($\varepsilon_M = 7$) and HfO_2, ($\varepsilon_H = 19$) respectively. A gate voltage $V_g = 0.5$ V yields a field $F = 400\,\mathrm{kV\,cm^{-1}}$. Our field modulation corresponds to a voltage difference of 20 V in the device of [14], giving a comparable shift of several meV for both the A^0 and the A^- peak. A Stark shift has been recently reported for the low-temperature photoluminescence of a MoS_2 monolayer sandwiched between two dielectrics [26]. The A peak position follows a hysteretic curve, which the authors ascribe to a joint effect of Stark effect and charge transfer with the top dielectric (Al_2O_3). Along most of their curve, our field modulation of $400\,\mathrm{kV\,cm^{-1}}$ would give a shift of a few meV in their device, consistent with our results. Please note that also in their data the linewidth changes, although they discuss only the peak shift.

The transverse field strength inside the MoS_2 layer may be inhomogeneous and deviate from equation (2) due to screening by charges from doping (during the synthesis or due to adsorption) and, for the orange, green, and cyan curves of figure 2(b), also from injection into the device. In the following, we make three assessments of the possible screening of the applied electric field by the charges present from doping: (i) estimating the electric field of a plane of the same surface charge density, (ii) estimating the Debye screening length, and (iii) discussing the effect of additional charges injected by switching the transistor to the *ON* state. The similar peak heights for the exciton and trion peaks in figures 2(h) and (i) suggest a doping level [14] of a few 10^{12} electrons $\mathrm{cm^{-2}}$. A plane of surface charge density $\sigma = 10^{12}$ electrons $\mathrm{cm^{-2}}$ generates an electric field of

$$F = \frac{\sigma e}{2\varepsilon_r \varepsilon_0} \tag{3}$$

$F = 130\,\mathrm{kV\,cm^{-1}}$. Hence, to completely screen 400 $\mathrm{kV\,cm^{-1}}$, all the electrons in the conduction band would have to form a surface charge at or even below the lower Sulphur plane of MoS_2. Such localization of electrons contradicts the more delocalized nature of the conduction band. Therefore, we conclude that the electrons present from doping may partially, but not completely screen the applied electric field.

A further assessment of the effectiveness of screening is provided by an estimate of the Debye screening length λ_D:

$$\lambda_D = \sqrt{\frac{\varepsilon_r \varepsilon_0 k_B T}{\rho e^2}} \tag{4}$$

We obtain $\lambda_D = 0.3$ nm, about half the thickness of the MoS_2 layer. If some of these charges are trapped, which is likely, they cannot contribute to the screening and λ_D is even longer [27]. Again, this estimate suggests that partial screening is possible, while complete screening is not. This assessment is further corroborated by the fact that injection of additional charges, with a density of the same order of magnitude as those from doping, results in a reduction but not in complete disappearance of the EA signal (figure 2(b)), again consistent with partial screening of the applied electric field. Please note that all production methods of MoS_2 (in particular also geological processes yielding the mineral molybdenite) customarily result in doped samples. Hence, published values for ε_r of MoS_2 already account for partial screening from a certain level of doping.

A linear shift in the applied field F is consistent with Stark effect originating from a permanent dipole moment or an induced dipole from a built-in electric field:

$$\Delta E = \overrightarrow{\Delta p} \cdot \vec{F} \tag{5}$$

With Δp being the difference in the dipole moment of the exciton (trion) and the neutral (charged) ground state. The shifts of a few meV correspond to differences in dipole moments between excited and ground states of a few Debye. Note that this is only a rough estimate obtained from the fits in figures 2(h) and (i). The MoS_2 monolayer itself should have no out-of-plane dipole moment for symmetry reasons, as has been confirmed by momentum-resolved photoluminescence spectroscopy [28]. Resolving the contradiction between the purely in-plane exciton dipole and the recently observed transverse Stark effect [25] is beyond the scope of the present paper. We can, however, briefly

discuss possible origins of either an out-of-plane dipole moment or a different mechanism for the field induced spectral shift. As discussed above, charges present in the doped MoS_2 monolayer can partially screen the transverse external field. The centre of the charge density is displaced from the Mo mirror plane as a function of the external field. This may affect both the bandgap and the exciton and trion binding energies. In particular, if the latter two change by different amounts, this results in a field-induced change in the distance between the exciton and trion peaks.

On the other hand, the spectral properties of MoS_2 are sensitive to the dielectric environment [29, 30]. In the momentum-resolved photoluminescence study MoS_2 was sandwiched between microscope oil and quartz, both dielectrics with relatively low ε_r. In our device the asymmetry is much larger (HfO_2 on one side of the monolayer, metal electrodes and air on the other), which may induce more significant transverse dipoles. In fact, EA spectroscopy is routinely used to characterize interface dipoles in heterostructure devices such as organic solar cells [31].

The dipole moment induced by the device structure can be manipulated by adsorbed molecules, since our experiments have been carried out in air. EA spectroscopy has been used to characterize the interface dipole between semiconductor nanocrystals and adsorbed dye molecules [32, 33]. We expect that the present paper will inspire similar work to study the effect of adsorbed molecules on MoS_2, whose effect on the electronic structure is hardly explored. Adsorbed molecules can also dope the channel [18] and thus change the ratio between the A^0 and A^- peaks. Simulations in the supplementary information (figure S1) show that for identical peak shifts the EA signal is strongest if A^- dominates the absorption spectrum, since it shifts more strongly. Device 1 (figure 1(d)) is p doped, as confirmed by the higher turn-on voltage. This lowers the A^- peak or even replaces it by an A^+ peak. From the above considerations, a lower A^- peak means a lower EA signal. An A^+ peak has never been reported in MoS_2, however, in WSe_2, compared to A^- it shows a smaller shift with field [34], in the opposite direction, which again lowers the EA. In figure 3 we show transmission and EA maps of both devices at the strongest EA peak (1.9 eV). Although we average over a spot size of $<$500 nm, we find that the signal between the two electrodes (a lower signal is also seen below the electrodes, probably due to multiple reflections in the substrate) varies between 0.15% and 0.22% for Device 1 and 0.40% and 0.52% for Device 2. The signal variation across the maps in Figure 3 does not follow the device geometry; hence, it must originate from some other heterogeneity, such as adsorbed molecules of varying density or charge puddles from doping. Hence EA microscopy—possibly pushed towards even higher resolution via near field scanning microscopy or stimulated emission depletion—may evolve into a tool for characterizing molecular adsorption and the micro-and nanostructure of doping in 2D materials.

Assessing the use in an EAM

Important performance figures for EAMs/EOMs are the insertion loss IL, the modulation depth MD, the device footprint A_d, and the switching energy per bit E_b. For typical applications an MD = 7 dB is required [3], while IL is typically around 1–2 dB. The device footprint of commercial devices typically exceeds 10^4 μm^2, but experimental devices with footprints ranging from 8 to 25 μm^2 have been realized [35, 36]. The switching energy per bit in state-of-the-art data centers is currently a few pJ bit^{-1}. However, to replace existing electrical interconnect technology, $E_b < 1$ fJ bit^{-1} is considered as the requirement for disruptive technology.

In the transmission geometry, as used for the experiments shown here, the IL is equal to the absorbance in the presence of the electric field and MD and IL relate straightforwardly to the absorbance A without field:

$$\mathrm{IL} + \mathrm{MD} = A \tag{6}$$

Hence, increasing the transmission in the presence of the electric field improves both performance figures together: it decreases IL and increases MD. We have shown switching from approximately 89% transmission to 89.5% transmission, corresponding to an insertion loss of 0.48 dB and a modulation depth of 0.02 dB. For comparison, a single layer of graphene, with the change in absorption caused by changes in the occupation of electronic levels rather than Stark effect, has negligible IL and an intrinsic upper limit of 0.10 dB for MD (2.3% transmission modulation [37]). To improve the performance of the 2d semiconductor device, the transmission in the presence of the electric field could be increased either if the A^0 and A^- peaks shifted more strongly (e.g. by using a material with larger intrinsic shift or a stronger modulated field), or if they were narrower with all other parameters equal or similar (see supplementary information, figure S1). Narrower peaks can be achieved either by cooling the device [38, 39] or by using other 2D compounds with narrower resonances, such as $MoSe_2$ [40]. The intrinsic performance limit would be a situation where in the presence of the electric field the A^0 and A^- peaks are completely separated, with a dip of almost zero absorbance in between them. In this limit, IL is negligible and MD of the monolayer is almost 0.5 dB, clearly exceeding the performance of graphene.

We assess attainable performance figures of the present device in two geometries: directly in transmission, as in the experiments shown above, and cladding a silicon waveguide to modulate the evanescent wave, as has been realized with grapheme [34, 41]. The graphene devices in the cladding configuration have IL = 3 dB, MD = 0.1 dB μm^{-1}, and A_d = 25 μm^2, which are among the best realized to date. As outlined above, MoS_2 performs similarly to graphene—4–5 times worse in the case of our non-optimised devices,

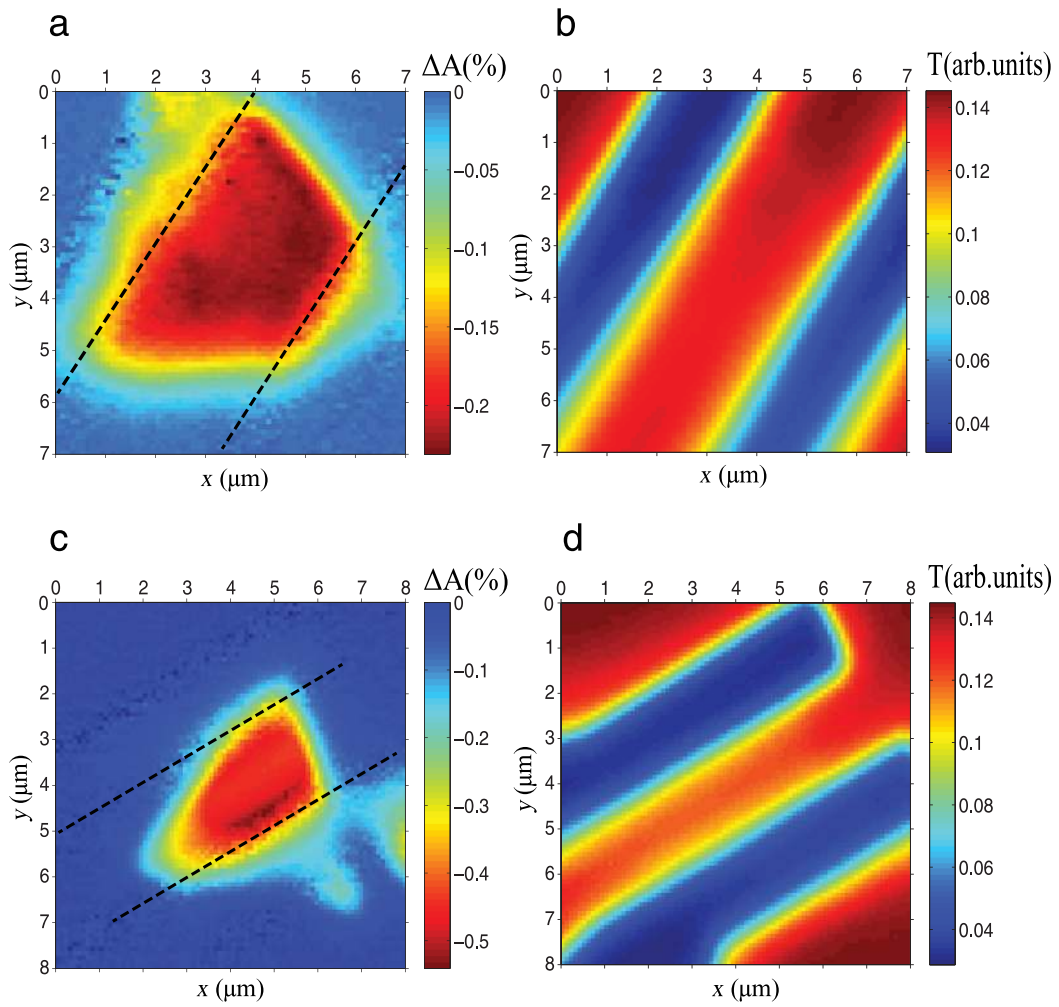

Figure 3. Electroabsorption and transmission maps of MoS_2 monolayer transistors. (a) and (b) Electroabsorption and transmission maps of device 1. (c) and (d) Electroabsorption and transmission maps of device 2. All measurements were performed at 650 nm, electroabsorption with a DC offset of −1 V and a modulated voltage $V_{pp} = 0.5$ V.

4–5 times better than graphene might be attainable. Hence, in this configuration, we can expect similar performance figures to the graphene devices.

An even more compact EAM can be envisaged by using directly the transmission geometry in which we performed our experiments. The device could be built to an overall thickness of 100 nm, reducing the device footprint to $< 1\ \mu m^2$. Assuming we can realistically attain MD > 0.2 dB for a monolayer, to achieve a viable MD of 7 dB, we would need a device with either 20–50 layers of MoS_2, or a multipass geometry (e.g. a monolayer inside a Fabry–Perot interferometer), or an even further increase of the light–matter interaction via the Purcell effect [42] or metallic nanostructures [43]. None of these strategies would increase the device footprint by more than a factor of 2. However, for a device consisting of 50 layers of MoS_2 in order to work at the same modulated electric field, V_{pp} would have to be increased to 1.8 V. The switching energy would then be $E_b = 1/2\ CV_{pp}^2 = 15$ fJ, for a device of $C = 14$ fF (assuming 30 nm HfO_2, 30 nm of MoS_2, and a device cross section of $3 \times 3\ \mu m$, as used here), while for the monolayer device $V_{pp} = 0.5$ V and $C = 50$ fF, yielding $E_b = 6$ fJ. Reducing the device cross section by one order of magnitude to the size of the focussed light spot (sub-μm) could proportionally reduce the device capacity and hence bring the switching energy to the sub-fJ bit^{-1} regime.

Conclusion

We have shown an unconventional electroabsorption effect in monolayer MoS_2 and ascribed it to linear field-induced shifts of the exciton and trion resonance peaks in opposite directions. The strength of the effect suggests that 2d semiconductors are excellent materials for EAMs. Monolayer MoS_2 shows its strongest EA signal at 1.9 eV (650 nm). However, there is a vast choice of 2D materials [44, 45] with bandgaps covering the whole range from 0 to beyond 5 eV, including the main telecom wavelengths (850–1550 nm). Compared to graphene, we envisage a possibly even shorter device with much lower power consumption due to the low off current [17]. Additionally, since the working principle is not based on changes in the population of levels, there is no excited state lifetime limit to the response time

[34, 40]. Such a device could be extremely compact and enable on-chip optical communication.

Acknowledgments

We are grateful for the inspiring discussions with S Bertolazzi, M Caironi, Ya A Gerasimenko, V V Kabanov, D Neumaier, V Perebeinos, J Strle, and T Heine. Device fabrication was carried out in the EPFL Center for Micro/Nanotechnology (CMI). We thank Z Benes (CMI) for technical support with e-beam lithography. The research leading to these results has received funding from the Marie-Curie ITN 'MoWSeS' (grant no. 317451),the European Union's Seventh Framework Programme FP7/2007-2013 under Grant Agreement No. 318804 (SNM) and the Swiss SNF Sinergia Grant no. 147607. We acknowledge funding by the EC under the Graphene Flagship (grant agreement no. 604391).

Author contributions

CG, AK, MRA, GL and DM planned and supervised the research. DD grew CVD MoS_2 samples on sapphire, DO, DV and Y-CK fabricated the devices, DO and DV performed electrical measurements on transparent transistors. DV and NM performed the electroabsorption measurements. DV and VVM analysed the data. CG and DV wrote the manuscript with critical input from all authors. Please contact daniele.vella@ijs.si or christoph.gadermaier@ijs.si for correspondence.

Competing financial interests

DV, CG, DO, AK, NM, MRA and GL have filed a UK patent 'Electro-optical Modulator based on a layered semiconductor crystal structure', GB 1600549.8.

References

[1] Miller D A B, Chemla D S, Damen T C, Gossard A C, Wiegmann W, Wood T H and Burrus C A 1984 Band-edge electroabsorption in semiconductor quantum wells: the quantum-confined Stark effect *Phys. Rev. Lett.* **53** 2173–6
[2] Miller D A B, Chemla D S, Damen T C, Gossard A C, Wiegmann W, Wood T H and Burrus C A 1985 Electric field dependence of optical absorption near the band gap of quantum-well structures *Phys. Rev.* B **32** 1043–60
[3] Reed G T, Mashanovich G, Gardes F Y and Thomson D J 2010 Silicon optical modulators *Nat. Photon.* **4** 518–26
[4] Mak K F and Shan J 2016 Photonics and optoelectronics of 2D semiconductor transition metal dichalcogenides *Nat. Photon.* **10** 216–26
[5] Sun Z P, Martinez A and Wang F 2016 Optical modulators with 2D layered materials *Nat. Photon.* **10** 227–38
[6] Wang Q H, Kalantar-Zadeh K, Kis A, Coleman J N and Strano M S 2013 Electronics and optoelectronics of two-dimensional transition metal dichalcogenides *Nat. Nanotechnol.* **7** 699–712
[7] Xia F, Wang H, Xiao D, Dubey M and Ramasubramaniam A 2014 Two-dimensional material nanophotonics *Nat. Photon.* **8** 899–907
[8] Ye Z, Cao T, O'Brien K, Zhu H, Yin X, Wang Y, Louie S G and Zhang X 2014 Probing excitonic dark states in single-layer tungsten disulphide *Nature* **513** 214–8
[9] Liu X, Galfsky T, Sun Z, Xia F N, Lin E C, Lee Y-H, Kena-Cohen S and Menon V M 2015 Strong light—matter coupling in two-dimensional atomic crystals *Nat. Photon.* **9** 30–4
[10] Sie E J, McIver J W, Lee Y-H, Fu L, Kong J and Gedik N 2015 Valley-selective optical Stark effect in monolayer WS_2 *Nat. Mater.* **14** 290–4
[11] Lopez-Sanchez O, Lembke D, Keyci M, Radenovic A and Kis A 2013 Ultrasensitive photodetectors based on monolayer MoS_2 *Nat. Nanotechnol.* **8** 497–501
[12] Xu H, Fathipour S, Kinder E W, Seabaugh A C and Fullerton-Shirey S K 2015 Reconfigurable ion gating of 2H-$MoTe_2$ field-effect transistors using poly(ethylene oxide)-$CsClO_4$ solid polymer electrolyte *ACS Nano* **9** 4900–10
[13] Mak K F, He K, Lee C, Lee G H, Hone J, Heinz T F and Shan J 2013 Tightly bound trions in monolayer MoS_2 *Nat. Mater.* **12** 207–11
[14] Chernikov A, van der Zande A M, Hill H M, Rigosi A F, Velauthapillai A, Hone J and Heinz T F 2015 Electrical tuning of exciton binding energies in monolayer WS_2 *Phys. Rev. Lett.* **115** 126802
[15] Zhang C, Wang H, Chan W, Manolatou C and Rana F 2014 Absorption of light by excitons and trions in monolayers of metal dichalcogenide MoS_2: experiments and theory *Phys. Rev.* B **89** 205403
[16] Lee C, Yan H, Brus L E, Heinz T F, Hone J and Ryu S 2010 Anomalous lattice vibrations of single-and few-layer MoS_2 *ACS Nano* **4** 2695–700
[17] Radisavljevic B, Radenovic A, Brivio J, Giacometti V and Kis A 2011 Single-layer MoS_2 transistors *Nat. Nanotechnol.* **6** 147–50
[18] Yue Q, Shao Z, Chang S and Li J 2013 Adsorption of gas molecules on monolayer MoS_2 and effect of applied electric field *Nanoscale Res. Lett.* **8** 425
[19] Sciascia C, Martino N, Schuettfort T, Watts B, Grancini G, Antognazza M R, Zavelani-Rossi M, McNeill C R and Caironi M 2011 Sub-micrometer charge modulation microscopy of a high mobility polymeric *n*-channel field-effect transistor *Adv. Mater.* **23** 5086–90
[20] Martino N, Fazzi D, Sciascia C, Luzio A, Antognazza M R and Caironi M 2014 Mapping orientational order of charge-probed domains in a semiconducting polymer *ACS Nano* **8** 5968–78
[21] Miller B, Parzinger E, Vernickel A, Holleitner A W and Wurstbauer U 2015 Photogating of mono- and few-layer MoS_2 *Appl. Phys. Lett.* **106** 122103
[22] Weiser G 1973 Modulation spectroscopy on anisotropic systems *Surf. Sci.* **37** 175–97
[23] Dumcenco D *et al* 2015 Large-area epitaxial monolayer MoS_2 *ACS Nano* **9** 4611–20
[24] Borzda T *et al* 2015 Charge photogeneration in few-layer MoS_2 *Adv. Funct. Mater.* **25** 3351–8
[25] Seyler K L, Schaibley J R, Gong P, Rivera P, Jones A M, Wu S, Yan J, Mandrus D G, Yao W and Xu X 2015 Electrical control of second-harmonic generation in a WSe_2 monolayer transistor *Nat. Nanotechnol.* **10** 407–11
[26] Klein J, Wierzbowski J, Regler A, Becker J, Heimbach F, Muller K, Kaniber M and Finley J J 2016 Stark effect spectroscopy of mono- and few-layer MoS_2 *Nano Lett.* **16** 1554–9
[27] Ghatak S, Pal A N and Ghosh A 2011 Nature of electronic states in atomically thin MoS_2 field-effect transistors *ACS Nano* **5** 7707–12
[28] Schuller J A, Karaveli S, Schiros T, He K, Yang S, Kymissis I, Shan J and Zia R 2013 Orientation of luminescent excitons in layered nanomaterials *Nature Nanotechnol.* **8** 271–6
[29] Buscema M, Steele G A, van der Zant H S J and Castellanos-Gomez A 2014 The effect of the substrate on the Raman and photoluminescence emission of single-layer MoS_2 *Nano Res.* **7** 561–71

[30] Ochedowski O, Marinov K, Scheuschner N, Poloczek A, Bussmann B K, Maultzsch J and Schleberger M 2014 Effect of contaminations and surface preparation on the work function of single layer MoS_2 *Beilstein J. Nanotechnol.* **5** 291–7
[31] Lane P A, Rostalski J, Giebeler C, Martin S J, Bradley D D C and Meissner D 2000 Electroabsorption studies of phthalocyanine/perylene solar cells *Sol. Energy Mater. Sol. Cells* **63** 3–13
[32] Nawrocka A and Krawczyk S 2008 Electronic excited state of alizarin dye adsorbed on TiO_2 nanoparticles: a study by electroabsorption (Stark effect) spectroscopy *J. Phys. Chem.* C **112** 10233–41
[33] Khoudiakov M, Parise A R and Brunschwig B S 2002 Interfacial electron transfer in Fe^{II}(CN)-sensitized TiO_2 nanoparticles: a study of direct charge injection by electroabsorption spectroscopy *J. Am. Chem. Soc.* **125** 4637–42
[34] Jones A M *et al* 2013 Optical generation of excitonic valley coherence in monolayer WSe_2 *Nat. Nanotechnol.* **8** 634–8
[35] Liu M, Yin X, Ulin-Avila E, Geng B, Zentgraf T, Ju L, Wang F and Zhang X 2011 A graphene-based broadband optical modulator *Nature* **474** 64–7
[36] Haffner C *et al* 2015 All-plasmonic Mach–Zehnder modulator enabling optical high-speed communication at the microscale *Nat. Photon.* **9** 525–9
[37] Nair R R, Blake P, Grigorenko A N, Novoselov K S, Booth T J, Stauber T, Peres N M R and Geim A K 2008 Fine structure constant defines visual transparency of graphene *Science* **320** 1308
[38] Moody G *et al* 2015 Intrinsic homogeneous linewidth and broadening mechanisms of excitons in monolayer transition metal dichalcogenides *Nat. Commun.* **6** 8315
[39] Korn T, Heydrich S, Hirmer M, Schmutzler J and Schuller C 2011 Low-temperature photocarrier dynamics in monolayer MoS_2 *Appl. Phys. Lett.* **99** 102109
[40] Tongay S, Zhou J, Ataca C, Lo K, Matthews T S, Li J B, Grossmann J C and Wu J K 2012 Thermally driven crossover from indirect toward direct bandgap in 2D semiconductors: $MoSe_2$ versus MoS_2 *Nano Lett.* **12** 5576–80
[41] Mohsin M, Schall D, Otto M, Noculak A, Neumaier D and Kurz H 2014 Graphene based low insertion loss electroabsorption modulator on SOI waveguide *Opt. Express* **22** 15292
[42] Gan X T *et al* 2013 Controlling the spontaneous emission rate of monolayer MoS_2 in a photonic crystal nanocavity *Appl. Phys. Lett.* **103** 181119
[43] Eda G and Maier S A 2013 Two-dimensional crystals: managing light for optoelectronics *ACS Nano* **7** 5660–5
[44] Nicolosi V, Chhowalla M, Kanatzidis M G, Strano M S and Coleman J N 2013 Liquid exfoliation of layered materials *Science* **340** 1226419
[45] Castellanos-Gomez A 2016 Why all the fuss about 2D semiconductors? *Nat. Photon.* **10** 202–4